frontiers | Frontiers in Signal Processing

TYPE Original Research
PUBLISHED 06 January 2026
DOI 10.3389/frsip.2025.1709070

OPEN ACCESS

EDITED BY
Le Liang,
Southeast University, China

REVIEWED BY
Zaid Albataineh,
Yarmouk University, Jordan
Ahmad Bazzi,
New York University Abu Dhabi, United Arab Emirates

*CORRESPONDENCE
Vimal Bhatia,
vbhatia@iiti.ac.in

RECEIVED 19 September 2025
REVISED 08 November 2025
ACCEPTED 18 November 2025
PUBLISHED 06 January 2026
CORRECTED 03 February 2026

CITATION
Bhatia V, Kumar R, Mitra R, Jain S, Shukla VB, Venkateswaran K and Krejcar O (2026) Convergence analysis of hyperparameter-free MCC-based channel estimation for mmWave MIMO systems.
Front. Signal Process. 5:1709070.
doi: 10.3389/frsip.2025.1709070

Convergence analysis of hyperparameter-free MCC-based channel estimation for mmWave MIMO systems

Vimal Bhatia[1,2,3]*, Rajat Kumar[1], Rangeet Mitra[4], Sandesh Jain[5], Vidya Bhasker Shukla[6], K. Venkateswaran[4] and Ondrej Krejcar[3]

[1]Soochow University, Suzhou, Jiangsu, China, [2]Department of Electrical Engineering, Indian Institute of Technology Indore, Indore, India, [3]Skoda Auto University, Mladá Boleslav, Czechia, [4]CMR Institute of Technology, Bengaluru, Karnataka, India, [5]Atal Bihari Vajpayee-Indian Institute of Information Technology and Management (ABV-IIITM), Gwalior, Madhya Pradesh, India, [6]University of Oulu, Oulu-FIN, Finland

Accurate channel-estimation algorithms are critical for enhancing the throughput of wireless communication systems, including millimetre wave (mmWave) multiple-input multiple-output (MIMO) systems, where precise channel knowledge enables reliable signal detection and beamforming. In practical wireless environments, impulsive non-Gaussian noise with unknown statistics often occurs due to electromagnetic interference and harsh propagation conditions, significantly degrading estimation accuracy and overall system performance. In this context, the maximum correntropy criterion (MCC) has emerged as an attractive solution for robust channel estimation that outperforms state-of-the-art algorithms. However, the MCC-based algorithm's performance is sensitive to the tuning of hyperparameters, which is challenging in the presence of non-Gaussian noise, such as impulsive noise (IN). Furthermore, a recent genre of kernel width sampling methods makes MCC hyperparameter-free and allows for asymptotic convergence to the squared-error performance of MCC with the ideal kernel width. To ensure their practical applicability, convergence analysis is essential to theoretically guarantee stability and performance under various IN scenarios. This study presents convergence analysis of hyperparameter-free MCC-based channel estimation for mmWave MIMO systems considering various IN scenarios. To validate the theoretical analysis, simulations are conducted on practical mmWave MIMO system models. Simulation results closely match the analytical findings, which confirms the accuracy and effectiveness of the analysis we here present.

KEYWORDS

channel estimation, millimetre wave, convergence analysis, hyperparameter-free maximum correntropy criterion, 5G/B5G

1 Introduction

Millimetre wave (mmWave) multiple-input multiple-output (MIMO) systems are crucial for next-generation wireless networks, offering high data throughput, extensive connectivity, and low latency (Hemadeh et al., 2017; Ali et al., 2020). These capabilities are essential for 5G, B5G, and future 6G networks due to their support for high-speed mobile broadband, ultra-reliable low-latency communications (URLLC), and massive machine-

type communications (mMTC) (Elbamby et al., 2018; Srivastava et al., 2019; Bhatia et al., 2019; Ali et al., 2020; Awan et al., 2017; Mitra et al., 2018). However, mmWave propagation has unique features that make precise channel estimation challenging (Heath et al., 2016). These include high route loss, low dispersion, and a preference for fewer spatial pathways. Real-world mmWave communication situations may experience non-Gaussian noise, including rapid signal fluctuations due to movement, blockage, air absorption, and device malfunctions (Zhao et al., 2013). As we move toward 6G, the operational spectrum is expanding to include mid-bands (7–15 GHz) for their favourable coverage-capacity trade-off alongside the continued use of mmWave (Saad et al., 2019). This development enables new paradigms such as integrated sensing and communication (ISAC), where channel state information is repurposed for high-resolution environmental imaging (Zhang et al., 2021; Bazzi et al., 2025). These advanced applications demand channel estimation that is not only accurate but also highly robust against the non-Gaussian noise prevalent in complex real-world deployments. MIMO systems started by using classic channel estimation methods such as least squares (LS) and minimum mean-square error (MMSE). However, these traditional methods exhibit significant limitations, especially in practical mmWave environments affected by impulsive and non-Gaussian noise. While non-parametric maximum likelihood (NPML) estimators provide robustness by modelling unknown noise distributions (Bhatia and Mulgrew, 2004), they suffer from high computational complexity, making them unsuitable for large-scale mmWave MIMO systems that require real-time processing. In contrast, the hyperparameter-free maximum correntropy criterion (MCC) has emerged as a low-complexity and effective alternative, as it captures higher-order error statistics and provides robustness against impulsive and non-Gaussian noise without the need for manual parameter tuning. Therefore, hyperparameter-free MCC offers a practical and efficient solution for robust channel estimation in mmWave MIMO systems, thus enabling reliable performance in challenging environments.

In traditional communication models, commonly represented additive white Gaussian noise (AWGN) is characterised as a normal distribution with a zero mean and constant variance. While this assumption is effective in several scenarios, it fails in environments with impulsive interference, such as urban wireless systems, where noise displays heavy-tailed characteristics (Selim et al., 2020b). As an example of heavy-tailed distributions, non-Gaussian impulsive noise (IN) is accurately characterised by the Bernoulli–Gaussian distribution (Selim et al., 2020b), which accounts for abrupt interference caused by environmental factors, electronic switching, and power fluctuations (Ghosh, 2002; Selim et al., 2020a; b).

In recent years, Bayesian-learning-based sparse recovery techniques have been explored for mmWave channel estimation, such as the iterative variational Bayes framework in Bazzi et al. (2016), where the channel is decomposed into angle-of-arrival (AoA) and angle-of-departure (AoD) components. However, these approaches generally assume a Gaussian prior/likelihood, which invalidates their scope to communication systems affected by IN with unknown statistics. To address robustness under such non-Gaussian conditions, the MCC has emerged as an effective alternative, as it captures higher-order error statistics beyond the second-order moments used in MMSE-based methods (Selim et al., 2020b). The MCC inherently enhances resilience to IN, improves convergence behaviour (Kumar et al., 2024) and preserves underlying channel–noise structure. Nevertheless, its performance is highly sensitive to the kernel width which varies with the noise characteristics and complicates receiver design (Ma et al., 2015; Chen et al., 2019). Recently, hyperparameter-free MCC algorithms (Mitra et al., 2021; Kumar et al., 2024) have de-necessitated adjustable kernel width selection by eliminating the need for hard-tuning and replacing it with hyperparameter-sampling, thereby simplifying receiver design. In detail, these methods utilise kernel sampling to asymptotically attain the performance of the MCC with an optimal kernel width, thereby alleviating the requirement for manual tuning. The adaptability of the hyperparameter-free MCC renders it especially suitable for real-time communication systems, where efficient and rapid estimation is essential.

Many current studies emphasise algorithm development instead of conducting a thorough analysis of critical parameters such as convergence behaviour, steady-state error performance, and robustness in the presence of various noise conditions (Kumar et al., 2024), which are essential for reliable deployment. This study addresses the gap by delivering a thorough performance analysis of hyperparameter-free-MCC-based channel-estimation in mmWave MIMO systems impaired by IN. We establish performance bounds, validate convergence properties, and compare efficiency with conventional MCC methods through theoretical derivations and simulations, which are not available in the literature. Our results clarify the practical feasibility of the hyperparameter-free MCC, particularly in real-world non-Gaussian noise situations, hence establishing it as a promising and versatile method for channel estimation for next-generation mmWave MIMO-based communication systems.

1.1 Contributions

Based on the above discussion, the key contributions of this work are summarised thus.

- Analysis of the convergence of hyperparameter-free MCC in the context of channel estimation for mmWave MIMO.
- An equation for the steady-state error is derived for the proposed algorithm, which is validated for various mmWave MIMO scenarios.
- A bound is derived for the step-size of the hyperparameter-free MCC to ensure convergence.

1.2 Notations

Vectors are represented by lowercase $\mathbf{a}$, while scalars are indicated by the letter a. Matrices are represented with uppercase letters such as $\mathbf{A}$. The notation $\mathbf{A}^{-1}$ denotes the inverse, $\mathbf{A}^{*}$ indicates the conjugate, $\mathbf{A}^{H}$ represents the Hermitian (conjugate transpose), and $\mathbf{A}^{T}$ signifies the transpose, using superscripts. The optimal value of a variable $(\cdot)$ is denoted as $(\cdot)_o$. Furthermore, the notation $(\cdot)^{(i)}$ represents the i^{th} term of the vector $(\cdot)$. $\text{vec}(\mathbf{A})$ represents the

vectorisation of the matrix $\mathbf{A}$. The trace, $\mathrm{Tr}(\cdot)$, sums the diagonal components of a matrix, while $\lambda_{\max}(\cdot)$ is the largest eigenvalue of a matrix. In this context, $\nabla(\cdot)$ represents the gradient of the function, while $\mathbb{E}[\cdot]$ signifies the statistical expectation. The l_p norm of a vector $\mathbf{x}$ can be given as $\|\mathbf{x}\|_p$.

2 System model

The transmitter and receiver design of the system comprises a transmitter fitted with N_{TX} transmit antennas and N_{RF} radio frequency (RF) chains and a receiver fitted with N_{RX} receive antennas and N_{RF} RF chains. Following the connection $N_d \le N_{RF} \le \min(N_{\mathrm{TX}}, N_{\mathrm{RX}})$, the number of RF chains is usually either less than or equal to the number of parallel data streams N_d. These streams represent a fundamental feature of hybrid beamforming systems, in which performance is maintained by using fewer RF chains than the total number of antennas, hence lowering hardware complexity. Combining the baseband precoder $\mathcal{F}_{\mathrm{BB}}$ with the RF precoder $\mathcal{F}_{\mathrm{RF}}$, a $N_{\mathrm{TX}} \times N_{RF}$ complex matrix forms the transmitted signal $\mathcal{F}$ (Alkhateeb et al., 2014). At the receiver, the RF combiner $\mathcal{W}_{\mathrm{RF}}$—a $N_{RF} \times N_{\mathrm{RX}}$ complex matrix—and the baseband combiner $\mathcal{W}_{\mathrm{BB}}$—a $N_{RF} \times N_d$ complex matrix—are utilised to analyse the received signal. Phase shifters enable the RF precoder and combiner to be constructed using only phase changes while maintaining constant signal magnitudes (Heath et al., 2016; Kumar et al., 2024). Effective beamforming made possible by this method enables the system to achieve high-performance communication in mmWave settings.

2.1 mmWave channel model

We investigate a dense urban non-line-of-sight (NLoS) scenario using the mmWave channel model. The channel is described as a narrowband geometric channel with a single propagation path between the transmitter and receiver, offered by each of the N scatterers. The channel matrix $\mathbf{H}$ is expressed using the standard geometric mmWave MIMO model (Heath et al., 2016):

$$\mathbf{H} = \sqrt{\frac{N_{\mathrm{TX}} N_{\mathrm{RX}}}{\eta}} \sum_{k=1}^{N} \rho_k \, \boldsymbol{\zeta}_{\mathrm{RX}}\left(\vartheta_k^{\mathrm{az}}, \vartheta_k^{\mathrm{el}}\right) \boldsymbol{\zeta}_{\mathrm{TX}}^{H}\left(\varphi_k^{\mathrm{az}}, \varphi_k^{\mathrm{el}}\right), \tag{1}$$

where, in Equation 1, ρ_k is the complex path gain of the k^{th} path and $(\cdot)^H$ denotes the Hermitian transpose. The parameters $\vartheta_k^{\mathrm{az}}$ and $\vartheta_k^{\mathrm{el}}$ represent the azimuth and elevation angles of arrival (AoAs), while φ_k^{az} and φ_k^{el} denote the azimuth and elevation angles of departure (AoDs), each ranging from $[-\pi/2, \pi/2]$. The factor η represents the average path loss between the transmitter (BS) and receiver (MS). Their respective antenna array response vectors to capture the 3D array geometry using Kronecker products may be written as

$$\boldsymbol{\zeta}_{\upsilon}\left(\alpha_k^{\mathrm{az}}, \alpha_k^{\mathrm{el}}\right) = \boldsymbol{\zeta}_{\upsilon}^{\mathrm{az}}\left(\alpha_k^{\mathrm{az}}\right) \otimes \boldsymbol{\zeta}_{\upsilon}^{\mathrm{el}}\left(\alpha_k^{\mathrm{el}}\right), \quad \upsilon \in \{\mathrm{TX}, \mathrm{RX}\}, \quad \alpha \in \{\varphi, \vartheta\}, \tag{2}$$

where, in Equation 2, $\otimes$ denotes the Kronecker product, and the vectors $\boldsymbol{\zeta}_{\upsilon}^{\mathrm{az}}(\cdot)$ and $\boldsymbol{\zeta}_{\upsilon}^{\mathrm{el}}(\cdot)$ represent the azimuth and elevation steering responses at the transmitter and receiver sides, respectively. They are mathematically expressed as

$$\boldsymbol{\zeta}_{\upsilon}^{\mathrm{az}}\left(\alpha_k^{\mathrm{az}}\right) = \frac{1}{\sqrt{N_{\upsilon}^{\mathrm{az}}}}\Big[1, \, e^{-j2\pi\frac{d}{\lambda}\cos\left(\alpha_k^{\mathrm{az}}\right)}, \, e^{-j2\pi\frac{d}{\lambda}2\cos\left(\alpha_k^{\mathrm{az}}\right)}, \ldots, \, e^{-j2\pi\frac{d}{\lambda}\left(N_{\upsilon}^{\mathrm{az}}-1\right)\cos\left(\alpha_k^{\mathrm{az}}\right)}\Big]^T, \tag{3}$$

where, in Equation 3, $d = \frac{\lambda}{2}$ denotes the inter-antenna spacing, and λ represents the carrier wavelength. A similar expression holds for the elevation steering vector $\boldsymbol{\zeta}_{\upsilon}^{\mathrm{el}}(\alpha_k^{\mathrm{el}})$ by replacing α_k^{az} with the elevation angle α_k^{el} and $N_{\upsilon}^{\mathrm{az}}$ with $N_{\upsilon}^{\mathrm{el}}$. The geometric channel model given in (1) can be equivalently expressed in the angular domain as $\mathbf{H} = \boldsymbol{\Lambda}_{\mathrm{RX}} \mathbf{H}_{\mathrm{a}} \boldsymbol{\Lambda}_{\mathrm{TX}}^{H}$, where $\boldsymbol{\Lambda}_{\mathrm{TX}}$ and $\boldsymbol{\Lambda}_{\mathrm{RX}}$ denote the transmit and receive array response dictionary matrices, respectively, while $\mathbf{H}_{\mathrm{a}}$ represents the beamspace channel matrix. Specifically, $\mathbf{H}_{\mathrm{a}}$ is defined as $\mathbf{H}_{\mathrm{a}} = \mathrm{diag}(\sqrt{\frac{N_{\mathrm{TX}} N_{\mathrm{RX}}}{\eta}} [\rho_1, \rho_2, \ldots, \rho_N]^T)$. The array response dictionary matrices are constructed as $\boldsymbol{\Lambda}_{\mathrm{RX}} = [\boldsymbol{\zeta}_{\mathrm{RX}}(\vartheta_1^{az}, \vartheta_1^{el}), \boldsymbol{\zeta}_{\mathrm{RX}}(\vartheta_2^{az}, \vartheta_2^{el}), \ldots, \boldsymbol{\zeta}_{\mathrm{RX}}(\vartheta_N^{az}, \vartheta_N^{el})]$, $\boldsymbol{\Lambda}_{\mathrm{TX}}^{H} = [\boldsymbol{\zeta}_{\mathrm{TX}}(\varphi_1^{az}, \varphi_1^{el}), \boldsymbol{\zeta}_{\mathrm{TX}}(\varphi_2^{az}, \varphi_2^{el}), \ldots, \boldsymbol{\zeta}_{\mathrm{TX}}(\varphi_N^{az}, \varphi_N^{el})]$ where $\boldsymbol{\zeta}_{\mathrm{TX}}(\varphi_i^{az}, \varphi_i^{el})$ and $\boldsymbol{\zeta}_{\mathrm{RX}}(\vartheta_i^{az}, \vartheta_i^{el})$ denote the transmit and receive steering vectors corresponding to the i^{th} azimuth–elevation AoD and AoA, respectively.

2.2 Formulation of the mmWave hybrid MIMO channel

The AoA and AoD are discretised into $G \ge \max(N_{\mathrm{TX}}, N_{\mathrm{RX}})$ evenly spaced points in the interval $[\frac{-\pi}{2}, \frac{\pi}{2})$. The AoD grid Ψ_{TX} and AoA grid Υ_{RX} are uniformly spaced and defined as

$$\Psi_{\mathrm{TX}} = \left\{\left(\varphi_m^{az}, \varphi_n^{el}\right) \; : \; \varphi_m^{az} = \frac{\pi(m-1)}{G}, \quad \varphi_n^{el} = \frac{\pi(n-1)}{G}, \quad 1 \le m, n \le G\right\}, \tag{4}$$

$$\Upsilon_{\mathrm{RX}} = \left\{\left(\vartheta_p^{az}, \vartheta_q^{el}\right) \; : \; \vartheta_p^{az} = \frac{\pi(p-1)}{G}, \quad \vartheta_q^{el} = \frac{\pi(q-1)}{G}, \quad 1 \le p, q \le G\right\}. \tag{5}$$

where in Equations 4, 5 the transmit and receive array response dictionaries (ARDs) are modelled using Kronecker products to jointly capture azimuth and elevation steering, given as $\boldsymbol{\Lambda}_{\mathrm{TX}}(\Psi_{\mathrm{TX}}) = \boldsymbol{\Lambda}_{\mathrm{TX}}^{az}(\varphi^{\mathrm{az}}) \otimes \boldsymbol{\Lambda}_{\mathrm{TX}}^{el}(\varphi^{\mathrm{el}})$ and $\boldsymbol{\Lambda}_{\mathrm{RX}}(\Upsilon_{\mathrm{RX}}) = \boldsymbol{\Lambda}_{\mathrm{RX}}^{az}(\vartheta^{\mathrm{az}}) \otimes \boldsymbol{\Lambda}_{\mathrm{RX}}^{el}(\vartheta^{\mathrm{el}})$. These matrices satisfy orthogonality conditions $\boldsymbol{\Lambda}_{\mathrm{TX}}(\Psi_{\mathrm{TX}})\boldsymbol{\Lambda}_{\mathrm{TX}}^{H}(\Psi_{\mathrm{TX}}) = \frac{G}{N_{\mathrm{TX}}}\mathbf{I}_{N_{\mathrm{TX}}}$ and $\boldsymbol{\Lambda}_{\mathrm{RX}}(\Upsilon_{\mathrm{RX}})\boldsymbol{\Lambda}_{\mathrm{RX}}^{H}(\Upsilon_{\mathrm{RX}}) = \frac{G}{N_{\mathrm{RX}}}\mathbf{I}_{N_{\mathrm{RX}}}$ (Srivastava et al., 2019). In the beamspace domain, the channel matrix $\mathbf{H}_s$ is represented as

$$\mathbf{H}_s = \boldsymbol{\Lambda}_{\mathrm{RX}}(\Psi_{\mathrm{RX}})\mathbf{H}_b\boldsymbol{\Lambda}_{\mathrm{TX}}^{H}(\Upsilon_{\mathrm{TX}}), \tag{6}$$

where in Equation 6, matrix $\mathbf{H}_b \in \mathbb{C}^{G \times G}$ denotes the diagonal channel matrix, which facilitates efficient channel estimation and signal processing. In practical 3D mmWave systems, antenna elements exhibit spatial correlation due to mutual coupling, limited inter-element spacing, and restricted angular spread in the propagation environment. To capture these effects, the conventional uncorrelated geometric channel model is extended to include both transmit and receive correlations using the Kronecker correlation model (Mitra and Bhatia, 2018; Forenza et al., 2007) as follows:

$$\mathbf{H}_{\mathrm{corr}} = \mathbf{R}_{\mathrm{RX}}^{1/2} \mathbf{H}_{\mathrm{s}} \mathbf{R}_{\mathrm{TX}}^{1/2}, \tag{7}$$

where, in Equation 7, $\mathbf{R}_{\mathrm{TX}} \in \mathbb{C}^{N_{\mathrm{TX}} \times N_{\mathrm{TX}}}$ and $\mathbf{R}_{\mathrm{RX}} \in \mathbb{C}^{N_{\mathrm{RX}} \times N_{\mathrm{RX}}}$ are the transmit and receive spatial correlation matrices, respectively. These matrices characterise the coupling effects among adjacent antenna elements at both link ends.

The correlation matrices are typically modelled as Toeplitz-structured matrices to represent spatial correlation among uniform planar array (UPA) elements. This Toeplitz exponential structure is widely adopted in the literature for accurately modelling the spatial correlation characteristics of UPA-based MIMO channels, owing to its ability to capture the exponential decay of correlation with antenna spacing (Van Zelst and Hammerschmidt, 2002; Čirkić and Larsson, 2014; Chikha et al., 2025).

$$\mathbf{R}_{\mathrm{TX}} = \mathrm{Toeplitz}\left(\left[1, \varrho, \varrho^2, \ldots, \varrho^{N_{\mathrm{TX}}-1}\right]\right), \tag{8}$$

$$\mathbf{R}_{\mathrm{RX}} = \mathrm{Toeplitz}\left(\left[1, \varrho, \varrho^2, \ldots, \varrho^{N_{\mathrm{RX}}-1}\right]\right), \tag{9}$$

where., in Equations 8, 9 $\varrho \in [0, 1]$ denotes the correlation coefficient that controls the strength of spatial correlation. The received signal matrix, denoted by $\mathbf{Y}$, incorporates the effect of the correlated 3D channel and is expressed in terms of the baseband and RF precoding matrices, together with the pilot matrix $\sqrt{P}\mathbf{I}_{N_{\mathrm{TX}}^{\mathrm{Beam}}}$. Specifically, the received signal model can be formulated as

$$\mathbf{Y} = \sqrt{P}\,\boldsymbol{\mathcal{W}}_{\mathrm{BB}}^{H}\boldsymbol{\mathcal{W}}_{\mathrm{RF}}^{H}\mathbf{H}_{\mathrm{corr}}\boldsymbol{\mathcal{F}}_{\mathrm{RF}}\boldsymbol{\mathcal{F}}_{\mathrm{BB}}\mathbf{I}_{N_{\mathrm{TX}}^{\mathrm{Beam}}} + \mathbf{W}, \tag{10}$$

where, in Equation 10, $\mathbf{W}$ denotes the additive noise matrix. To facilitate channel estimation, the received signal matrix $\mathbf{Y}$ must be vectorised. After applying the property $\mathrm{vec}(\mathbf{ABC}) = (\mathbf{C}^T \otimes \mathbf{A})\,\mathrm{vec}(\mathbf{B})$, the received signal can be expressed as

$$\mathbf{y} = \mathrm{vec}(\mathbf{Y}) = \sqrt{P}\bar{\mathbf{Z}}\mathbf{h}_{\mathrm{eff}} + \mathbf{w}, \tag{11}$$

where, in Equation 11, $\mathbf{y} \in \mathbb{C}^{N_{\mathrm{RX}}^{\mathrm{Beam}} N_{\mathrm{TX}}^{\mathrm{Beam}} \times 1}$ is the vectorised received signal, $\mathbf{h}_{\mathrm{eff}} = \mathrm{vec}(\mathbf{H}_{\mathrm{corr}}) = (\mathbf{R}_{\mathrm{TX}}^{1/2T} \otimes \mathbf{R}_{\mathrm{RX}}^{1/2})(\boldsymbol{\Lambda}_{\mathrm{TX}}^{*} \otimes \boldsymbol{\Lambda}_{\mathrm{RX}})\mathbf{h}_b \in \mathbb{C}^{N_{TR}N_{RX} \times 1}$, $\mathbf{h}_b = \mathrm{vec}(\mathbf{H_b})$ represents the beamspace channel vector, and $\bar{\mathbf{Z}} = \boldsymbol{\mathcal{F}}_{\mathrm{BB}}^{T}\boldsymbol{\mathcal{F}}_{\mathrm{RF}}^{T} \otimes \boldsymbol{\mathcal{W}}_{\mathrm{BB}}\boldsymbol{\mathcal{W}}_{\mathrm{RF}} \in \mathbb{C}^{N_{TX}^{\mathrm{Beam}} N_{RX}^{\mathrm{Beam}} \times N_{RX}N_{TX}}$ is the sensing matrix. The vectorised noise, $\mathbf{w} = \mathrm{vec}(\mathbf{W})$, follows a Gaussian–Bernoulli distribution, reflecting the characteristics of impulsive noise (Selim et al., 2020b). Its probability density function (PDF) of n follows a bimodal Gaussian distribution, as

$$p(w) = (1 - p)\mathcal{N}(0, \sigma_w^2) + p\mathcal{N}(0, \Gamma\sigma_w^2), \tag{12}$$

where, Equation 12, $\mathcal{N}(\mu, \sigma^2)$ represents a normal distribution with mean μ and variance σ^2. The parameters p and Γ define the characteristics of the impulsive noise model, where Γ represents the noise variance scaling factor and p indicates the probability of encountering the high-variance noise component.

3 Review of hyperparameter-free MCC

Information theoretic learning (ITL)-based adaptive signal processing methods are viable for generic signal processing over scenarios impaired by non-Gaussian additive distortions (Chen et al., 2013). In the context of hyperparameter-free ITL-based channel estimation over impulsive noise, this section first reviews two recent ITL-based strategies among the existing research: the recently proposed MCC and the hyperparameter-free MCC. In further sections, the convergence of the hyperparameter-free MCC is analysed.

3.1 Review of MCC-based channel estimation

In this section, we review a channel estimation method based on MCC derived in Kumar et al. (2024). We denote the auto-covariance matrix $\mathbf{C}$ as $\mathbf{C} = \mathbb{E}\left\{\bar{\mathbf{Z}}^H(n)\bar{\mathbf{Z}}(n)\right\} \in \mathbb{C}^{G^2 \times G^2}$ and the cross-covariance vector $\mathbf{b}$ as $\mathbf{b} = \mathbb{E}\left\{\bar{\mathbf{Z}}^H(n)\mathbf{y}(n)\right\} \in \mathbb{C}^{G^2 \times 1}$. The error term $\mathbf{e}$ is defined as $\mathbf{e}(n) = \mathbf{b} - \mathbf{C}\hat{\mathbf{h}}_b(n)$. The MCC-based cost function is formulated as

$$J_{MCC}(n) = \mathbb{E}\left\{\sum_{i=1}^{N} \exp\left(-\gamma|\mathbf{e}^{(i)}(n)|^2\right)\right\}, \tag{13}$$

where the parameter γ serves as the hyperparameter for the MCC criterion and is typically determined using various heuristic approaches. By applying the steepest descent method to Equation 13, the update equation for the MCC algorithm is derived as

$$\hat{\mathbf{h}}_b^{(i)}(n+1) = \hat{\mathbf{h}}_b^{(i)}(n) + \mu \exp\left(-\gamma|\mathbf{e}^{(i)}(n)|^2\right)\mathbf{e}^{(i)}(n), \tag{14}$$

where, in Equation 14, μ denotes the step size. The MCC method is resilient to non-Gaussian noise by approximating R-nyi's α order information potential. Nonetheless, the performance of MCC mostly relies on the "best value," γ, which is chosen via heuristic techniques. We next propose a hyperparameter-free variation of MCC to overcome this restriction.

3.2 Review of hyperparameter-free MCC-based channel estimation

In this section, we review the recently formulated hyperparameter-free MCC (Kumar et al., 2024). We first form a vector $\mathbf{l}(n)$ as

$$\mathbf{l}(n) = \mathbf{C}(n)\hat{\mathbf{h}}_b(n).$$

Then in (Equation 14), RFF mapping approximates the exponential term of the MCC cost function (Mitra et al., 2021):

$$\exp\left(-\gamma|\mathbf{e}^{(i)}|^2\right) = \Phi\left(\mathbf{b}^{(i)}\right)^{\top}\Phi\left(\mathbf{l}^{(i)}\right), \tag{15}$$

where, in Equation 15, $\Phi(.)$ is the hyperparameter-free RFF mapping derived in Mitra et al. (2022), which can be provided as

$$\Phi(\mathbf{x}) = \sqrt{\frac{2}{n_G}}\begin{bmatrix} \cos\left(h_1\boldsymbol{\xi}_1^T\left[\Re[\mathrm{x}]^T\Im[\mathrm{x}]^T\right]^T + b_1\right) \\ \vdots \\ \cos\left(h_{n_G}\boldsymbol{\xi}_{n_G}^T\left[\Re[\mathrm{x}]^T\Im[\mathrm{x}]^T\right]^T + b_{n_G}\right) \end{bmatrix}, \tag{16}$$

where, in Equation 16, $\boldsymbol{\xi}_i \sim \mathcal{N}(0, \mathbf{I}_{2n})$ and $\mathbf{b}_i \sim U[0, 2\pi]$ where $U[a, b]$ signifies a uniform distribution inside the closed interval $[a, b]$. The kernel parameters $\mathbf{h}_i$ for each term are drawn from a Gamma distribution, $\mathbf{h}_i \sim \Gamma(\alpha_i, \beta_i)$. The parameters α_i and β_i are determined as per Mitra et al. (2021).

$$\alpha_i = \frac{1}{2}, \quad \beta_i = \frac{\epsilon}{8\pi^2\alpha_i}. \tag{17}$$

Notably, in Equation 17, α_i and β_i are not considered hyperparameters as they are determined using explicit formulae for initialisation (Mitra et al., 2021). Additionally, the approximation error decreases with increasing n_G (Rahimi and Recht, 2007), so n_G is also not a hyperparameter. We rewrite the adaptive equation for hyperparameter-free MCC using this mapping as follows:

$$\hat{\mathbf{h}}_b^{(i)}(n+1) = \hat{\mathbf{h}}_b^{(i)}(n) + \mu\,\Phi\left(\mathbf{b}^{(i)}\right)^{\top}\Phi\left(\mathbf{l}^{(i)}\right)\mathbf{e}^{(i)}(n), \tag{18}$$

where, in Equation 18, μ denotes the step size. The next section provides a detailed convergence analysis of the hyperparameter-free MCC algorithm.

4 Derivation of convergence analysis

This section contributes to the theoretical analysis of the steady-state behaviour of the hyperparameter-free MCC-based channel-estimation algorithm for mmWave MIMO. The energy conservation analysis relation is widely applied to convergence analysis in adaptive filtering theory. We denote $\tilde{\mathbf{e}}(n) = 2\mathbf{C}\tilde{\mathbf{h}}(n) = \sum_{\forall i}\mathbf{q}_i\lambda_i\mathbf{q}_i^{\top}\tilde{\mathbf{h}}(n)$ as the estimation error, $\mathbf{q}_i$ denote the i^{th} eigenvector, and λ_i signify the i^{th} eigenvalue of $\mathbf{C}$. In this context, $\tilde{\mathbf{h}}(\mathbf{n}) = \mathbf{h}_o - \hat{\mathbf{h}}(n)$ indicates the error vector in the i^{th} iteration, with $\mathbf{h}_o$ denoting the optimal value of $\mathbf{h}$. The i^{th} tuple of the weight vector $\hat{\mathbf{h}}^{(i)}(n)$ is updated using Equation 18 as follows, and after subtracting the true parameter vector $\mathbf{h}_o$ both sides, we can then represent the following update equation:

$$\hat{\mathbf{h}}_b^{(i)}(n+1) = \hat{\mathbf{h}}_{\mathbf{b}}^{(i)}(n) + \mu\underbrace{\Phi\left(b^{(i)}\right)^{T}\Phi\left(\mathbf{l}^{(i)}\right)}_{\Theta^{(i)}(\infty)\to 1}\mathbf{e}^{(i)}(n), \tag{19}$$

where, in Equation 19, $\Phi(\cdot)$ denotes the random-feature mapping, μ is the step size, and Θ represents the random-feature inner product approximating the kernel function $\exp(-\gamma|\mathbf{e}^{(i)}(n)|^2)$ (Mitra et al., 2021). Subtracting $\mathbf{h}_o$ from both sides of 19 gives the weight error update equation

$$\tilde{\mathbf{h}}^{(i)}(n+1) = \tilde{\mathbf{h}}^{(i)}(n) - \mu\left(\tilde{\mathbf{e}}^{(i)}(n) + \mathbf{w}\right)\cdot\Theta^{(i)}(n), \tag{20}$$

where $\mathbf{w}$ denotes the noise component and $\tilde{\mathbf{e}}^{(i)}(n) = \lambda_i\tilde{\mathbf{h}}^{(i)}(n)$.

4.1 Step-size range for convergence

To ensure convergence of the iterative process, the squared norm of the updated Equation 20 must satisfy the following condition:

$$|\tilde{\mathbf{h}}^{(i)}(n+1)|^2 \approx |\tilde{\mathbf{h}}^{(i)}(n)|^2\left(1 + \frac{\mu^2\lambda_i^2}{4} - 2\mu\lambda_i\Theta^{(i)}(n)\right) + \frac{\mu^2\left[(1-p)\sigma_w^2 + p\Gamma\sigma_w^2\right]}{4}. \tag{21}$$

For convergence, it is necessary that

$$0 < \left(1 + \frac{\mu^2\lambda_i^2}{4} - 2\mu\lambda_i\Theta^{(i)}(n)\right) < 1,$$

which ensures that the update reduces the weight error over time. Simplifying this inequality yields leads to Equation 22 below:

$$0 < \frac{\mu^2\lambda_i^2}{4} < 2\mu\lambda_i\Theta^{(i)}(n), \qquad 0 < \mu < \frac{8\Theta^{(i)}(n)}{\lambda_i}. \tag{22}$$

To guarantee convergence for all modes of the system, we consider the most restrictive case by using the maximum eigenvalue $\lambda_{\max}$, resulting in the general stability bound:

$$0 < \mu < \frac{8\Theta^{(i)}}{\lambda_{\max}}, \tag{23}$$

where, in Equation 23, $\lambda_{\max}$ is the maximum eigenvalue of the system. This condition ensures stability and prevents divergence during the learning process. To incorporate the stochastic behaviour of Θ, we assume the error sequence $\mathbf{e}$ to be monotonically decreasing for a given step-size range and denote the value of its first element as $\mathcal{M}$ such that $\sigma_e^2 \le \mathcal{M}$. Under this assumption, the bounds on $\mathbb{E}[\Theta]$ are given by

$$\frac{1}{\sqrt{1+\gamma_o\mathcal{M}}} \le \mathbb{E}[\Theta] \le 1, \tag{24}$$

where, in Equation 24, γ_o is the optimal kernel-width parameter as defined in Mitra et al. (2021). Accordingly, the rectified step-size range ensuring mean-square stability, based on the 3σ spread of e, can be expressed as below in Equation 25:

$$0 < \mu < \frac{8}{\lambda_{\max}}\left[\frac{1}{\sqrt{1+\gamma_o\mathcal{M}}} - 3\times\sqrt{\frac{1}{(1+4\gamma_o\mathcal{M})^{1/2}} - \frac{1}{1+2\gamma_o\mathcal{M}}}\right]. \tag{25}$$

In the context of the MCC criterion using γ_o, we invoke an instantaneous "rough" approximation for regular data and outliers (demarcated by the variable $\mathcal{E}$):

$$\begin{aligned}\Theta = \exp\left(-\gamma_o e^2\right) &\approx 1, \quad \text{if } |e| < \mathcal{E},\\ \Theta &\approx 0, \quad \text{if } |e| > \mathcal{E}.\end{aligned} \tag{26}$$

Since most of the adaptations are from regular data (due to the inherent outlier-suppressing capacity of MCC), the transient response is governed by $\gamma_o\mathcal{M} \ll 1$. This yields the following simplified range for the step-size μ as seen from Equation 26:

$$0 < \mu < \frac{8}{\lambda_{\max}}, \tag{27}$$

since $\mathbb{E}[\Theta^{(i)}] \to 1$ and $\mathrm{Var}[\Theta^{(i)}] \to 0$ for $\gamma_o\mathcal{M} \ll 1$ as concluded from (Equation 25). This formulation provides a statistically robust condition for mean-square stability, even under impulsive noise environments.

4.2 Steady-state behaviour

At steady state $(n \to \infty)$, the weight vector $\hat{\mathbf{h}}^{(i)}(\infty)$ converges to a constant value, and the update term becomes negligible.

Mathematically, this implies $\tilde{\mathbf{h}}^{(i)}(n+1) \approx \tilde{\mathbf{h}}^{(i)}(n)$ the squared norm of $\tilde{\mathbf{h}}^{(i)}(\infty)$ satisfies

$$|\tilde{\mathbf{h}}^{(i)}(\infty)|^2\left(2\mu\lambda_i\Theta^{(i)}(\infty) - \frac{\mu^2\lambda_i^2}{4}\right) = \frac{\mu^2\left[(1-p)\sigma_w^2 + p\Gamma\sigma_w^2\right]}{4}. \quad (28)$$

Dividing both sides of Equation 28 by $(2\mu\lambda_i\Theta^{(i)}(\infty) - \frac{\mu^2\lambda_i^2}{4})$ gives Equation 21, isolating $|\tilde{\mathbf{h}}^{(i)}(\infty)|^2$.

$$|\tilde{\mathbf{h}}^{(i)}(\infty)|^2 = \frac{\frac{\mu^2\left[(1-p)\sigma_w^2+p\Gamma\sigma_w^2\right]}{4}}{\left(2\mu\lambda_i\Theta^{(i)}(\infty) - \frac{\mu^2\lambda_i^2}{4}\right)}. \quad (29)$$

From Equation 29, the mean squared deviation (MSD), which quantifies the steady-state error, is given by

$$\text{MSD} = \sum_{\forall i} \frac{\mu\frac{(1-p)\sigma_w^2+p\Gamma\sigma_w^2}{4}}{2\lambda_i\Theta^{(i)}(\infty) - \frac{\mu\lambda_i^2}{4}} \approx \sum_{\forall i} \frac{\mu\frac{(1-p)\sigma_w^2+p\Gamma\sigma_w^2}{4}}{8\lambda_i - \mu\lambda_i^2}, \quad (30)$$

where covariance matrix $\mathbf{C}$ is characterised by the eigenvalues $\{\lambda_i\}$, which directly influence both the convergence condition and the steady-state MSD, as reflected in the derived analytical expressions.

In the next section, we validate Equation 30 through computer simulations assuming practical mmWave MIMO channels. From the above analysis, we can conclude the following salient points.

- From our analysis, it is guaranteed that the proposed algorithm approaches the converged MSD in (Equation 30) without depending on hyperparameters specific to noise statistics.
- We are aware of the performance analysis of MCC variants, either with variable spread factor or using rules of thumb (Ma et al., 2015). In this context, our contribution/analysis is novel as we do not depend on accurate spread factor initialisations in our formulation/convergence analysis; rather, we sample it according to $\Gamma[\alpha, \beta]$.

It is noteworthy that α, β themselves are not hyperparameters, as they are explicit formulae to initialise them (Mitra et al., 2021). Furthermore, the approximation error monotonously decreases with an increase in n_G (Rahimi and Recht, 2007); thus, n_G is also not a hyperparameter.

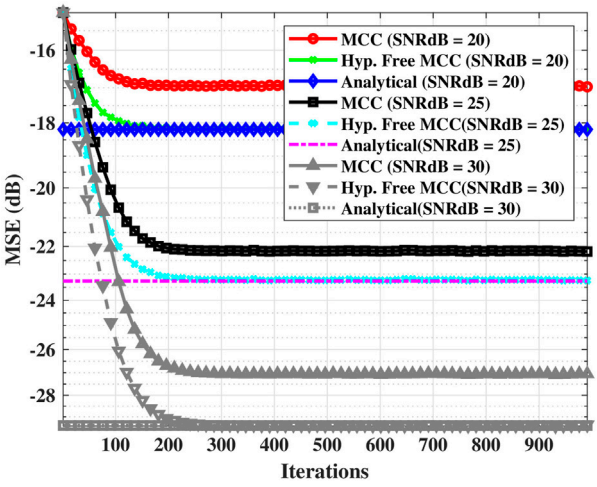

FIGURE 1
MSE vs. iterations for MCC and hyperparameter-free MCC (32 × 32 MIMO, $N_{RF} = 8$, $N = 2$, $p = 0.1$, and $\Gamma = 10$); step size $\mu = 0.003$ lies within the analytical bound (Equation 27).

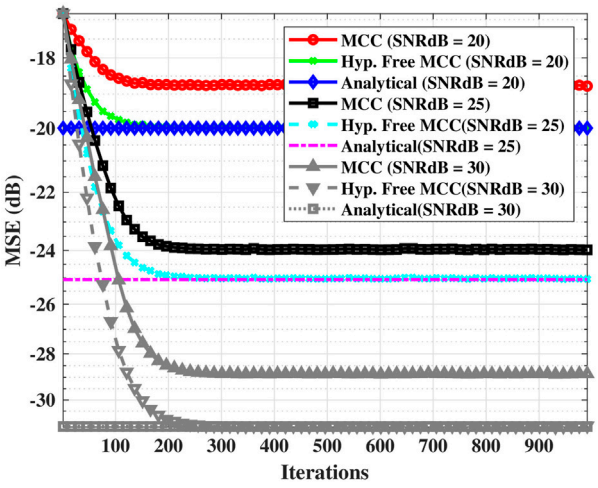

FIGURE 2
MSE vs. iterations for MCC and hyperparameter-free MCC (64 × 64 MIMO, $N_{RF} = 8$, $N = 2$, $p = 0.1$, and $\Gamma = 10$); step size $\mu = 0.003$ lies within the analytical bound (Equation 27).

5 Simulation results

This section validates the convergence analysis of the proposed hyperparameter-free MCC method for mmWave MIMO channel estimation. We run the simulations under various signal-to-noise ratio (SNR) levels and MIMO orders to assess the accuracy, generality, and robustness of hyperparameter-free MCC and to validate the convergence analysis. The simulation setup consists of an mmWave MIMO system with $N = 8$ RF chains, $N_{TX} = 32$ transmit antennas, and $N_{RX} = 32$ receive antennas, as well as an extended case with $N_{TX} = 64$ transmit antennas and $N_{RX} = 64$ receive antennas. The channel is distinguished as a narrowband geometric channel with $N = 2$ scatterers where the AoA and the AoD are evenly distributed in the interval $[0, \pi)$. As described in Section 2, the noise is expressed as a bimodal Gaussian distribution whereby the probability p of meeting high-variance noise components changes across several situations.

5.1 MSE vs. iterations for different μ, p, N, and Γ

In the first scenario, we examine a situation with a high probability of high-variance noise $(p = 0.1)$ together with a

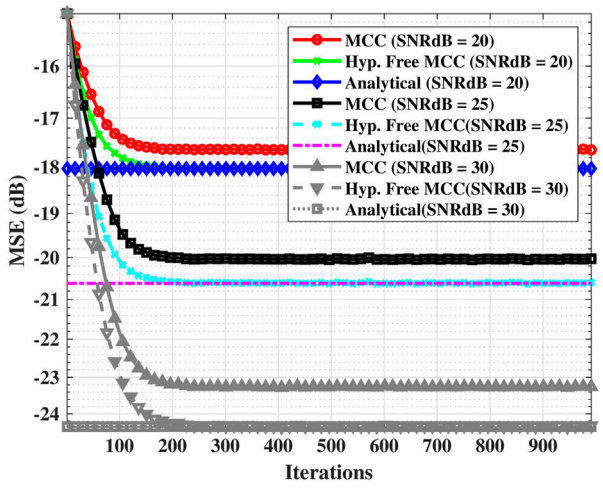

FIGURE 3
MSE vs. iterations for MCC and hyperparameter-free MCC (32 × 32 MIMO, N_{RF} = 8, N = 2, p = 0.01, and Γ = 100); step size μ = 0.007 lies within the analytical bound (Equation 27).

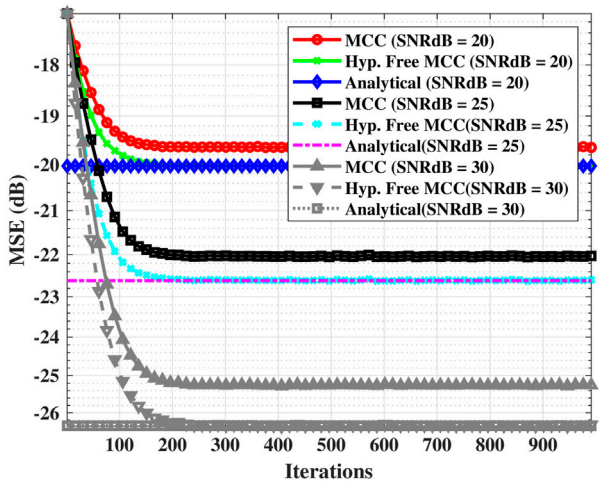

FIGURE 4
MSE vs. iterations for MCC and hyperparameter-free MCC (64 × 64 MIMO, N_{RF} = 8, N = 2, p = 0.01, and Γ = 100); step size μ = 0.007 lies within the analytical bound (Equation 27).

modest noise variance scaling factor (Γ = 10) (Selim et al., 2020b). Figures 1, 2 illustrate the relationship between MSE and the number of iterations at SNR levels of 20 dB, 25 dB, and 30 dB for both 32 × 32 and 64 × 64 MIMO configurations. The results show that, with rising SNR, the proposed hyperparameter-free MCC method approaches an MSE close to the noise floor given by (30). Furthermore, there is substantial agreement between the analytical and the simulated MSE in the high SNR regime, which reinforces the analytical results presented in the previous section.

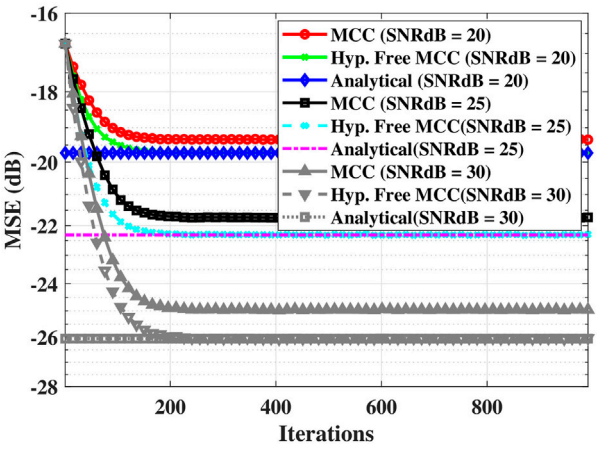

FIGURE 5
MSE vs. iterations for MCC and hyperparameter-free MCC (64 × 64 MIMO, N_{RF} = 8, N = 4, p = 0.01, and Γ = 100); step size μ = 0.007 lies within the analytical bound (Equation 27).

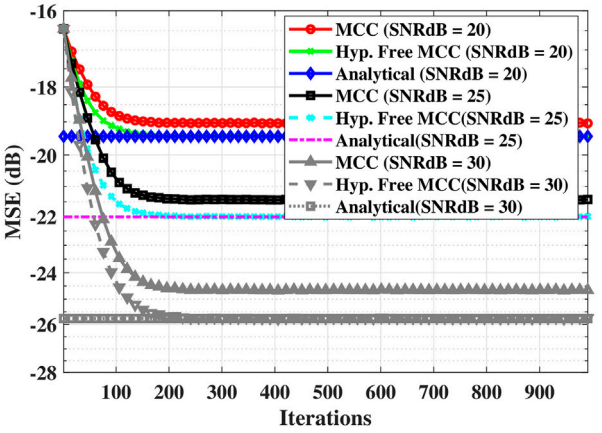

FIGURE 6
MSE vs. iterations for MCC and hyperparameter-free MCC (64 × 64 MIMO, N_{RF} = 8, N = 5, p = 0.01, and Γ = 100); step size μ = 0.007 lies within the analytical bound (Equation 27).

Consequently, in Figures 3, 4 we investigate the settings of Scenario 2 for (p = 0.01) and Γ = 100. Figures 3, 4 display the MSE vs. iterations for SNR levels of 20 dB, 25 dB, and 30 dB for both 32 × 32 and 64 × 64 MIMO configurations. Once again, as in Figures 1, 2, we observe the achievement of hyperparameter-free MCC to the analytical noise floor in (Equation 30).

In Scenario 3, Figures 4–6 analyse the effect of channel sparsity on the analytical MSE bound by varying the number of propagation paths as $N = \{2, 4, 5\}$ while maintaining the same angular spread. The results indicate that as the number of paths increases (i.e., sparsity decreases), the steady-state MSE remains nearly constant, validating the robustness of the analytical bound under different sparsity levels. Furthermore, we examine the impact of the step-size parameter on convergence behaviour in Figure 7, which presents the MSE *versus* iteration performance for step sizes chosen

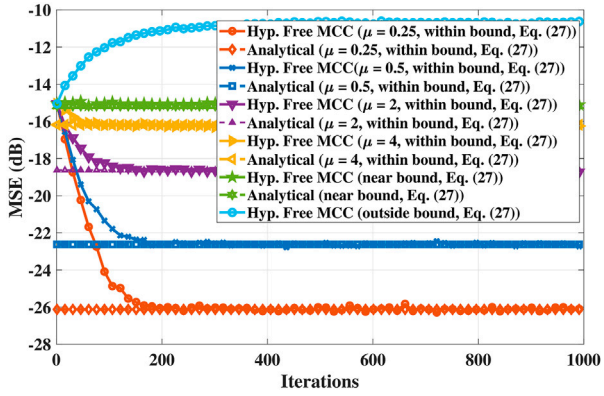

FIGURE 7
Convergence behaviour of the hyperparameter-free MCC for 32 × 32 MIMO MSE for various step sizes; (μ) lies within, near, and outside the analytical bound (Equation 27); (N_{RF} = 8, N = 2, p = 0.1, and Γ = 50).

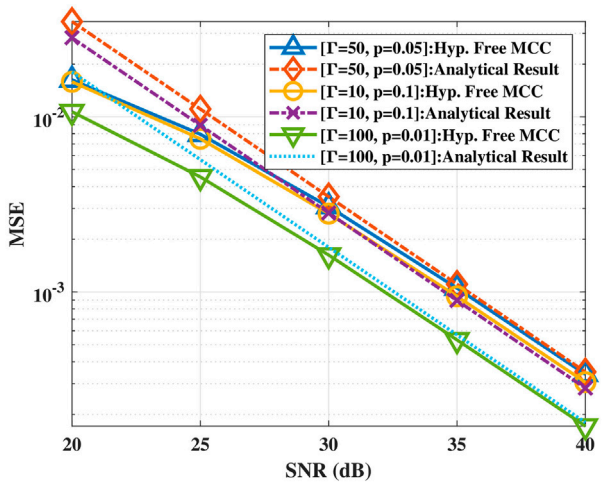

FIGURE 8
MSE vs. SNR for MCC and hyperparameter-free MCC (32 × 32 MIMO, N_{RF} = 8, and N = 2); step size μ = 0.003 lies within the analytical bound (Equation 27).

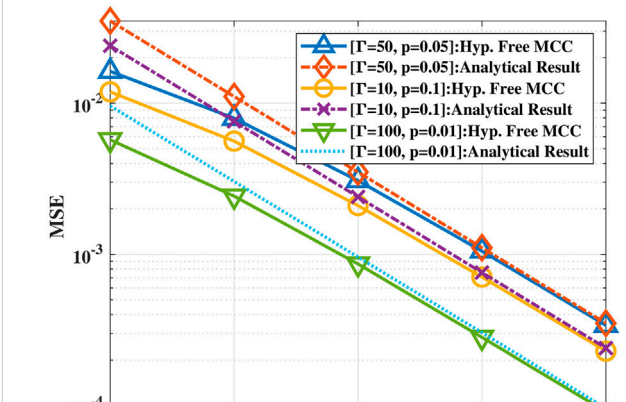

FIGURE 9
MSE vs. SNR for MCC and hyperparameter-free MCC (32 × 32 MIMO, N_{RF} = 8, and N = 2); step size μ = 0.003 lies within the analytical bound (Equation 27).

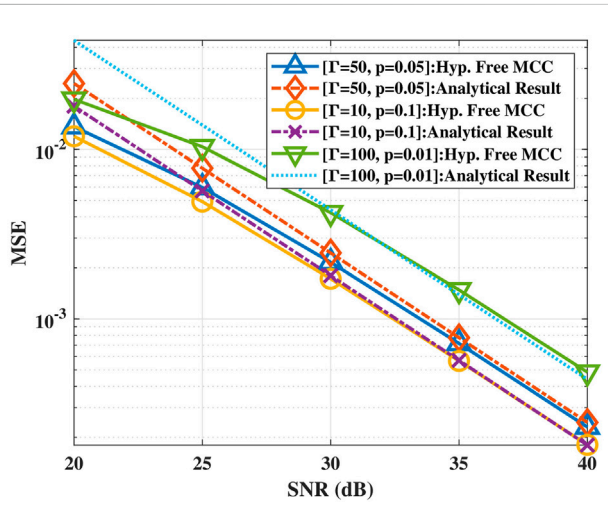

FIGURE 10
MSE vs. SNR for MCC and hyperparameter-free MCC (32 × 32 MIMO, N_{RF} = 8, and N = 2); step size μ = 0.007 lies within the analytical bound (Equation 27).

within the bound, near the boundary, and outside the bound as defined by the analytical condition in (Equation 27). The results clearly demonstrate that the algorithm converges smoothly when μ lies within the derived range, exhibits marginal stability near the boundary, and diverges when μ exceeds the upper limit, thereby confirming the validity of the theoretical step-size stability criterion.[1] In summary, the effectiveness of the suggested analysis is underlined by the close agreement between the simulated and analytical error floor, enforcing the generality of these results.

5.2 MSE vs. SNR for different (μ)

For μ = 0.003, Figures 8, 9 show the MSE performance. Figures 8, 9 reveal that the MSE falls as the SNR rises. Particularly at reduced SNRs, the figures for various gamma values (Γ = 10, 50, 100) indicate that at low/moderate SNR, the hyperparameter-free MCC achieves improved performance compared to the derived bound in Equation 30. This artefact is clearly visible as we vary (p = 0.1, 0.05, 0.01) and change μ = 0.007 in Figures 10, 11. The close match of the analytical MSE with the simulated MSE at high SNR regime validates the theoretical analytical result in (Equation 30) (in other words, (Equation 30) is a max-entropy upper bound for a given covariance ($(1-p)\sigma_w^2 + p\Gamma\sigma_w^2$(Cover and Thomas, 1991)).

1 We have noticed this trend for various values of p, Γ, N, which we do not show in this manuscript for conciseness of presentation.

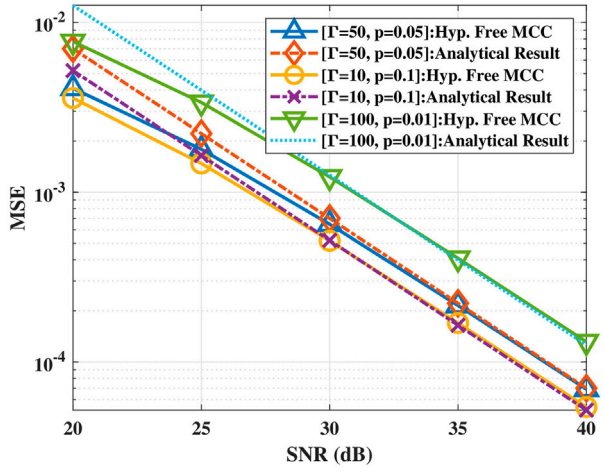

FIGURE 11
MSE vs. SNR for MCC and hyperparameter-free MCC (64 × 64 MIMO, N_{RF} = 8, and N = 2); step size μ = 0.007 lies within the analytical bound (Equation 27).

6 Conclusion

This paper analyses the convergence of hyperparameter-free MCC techniques for channel estimation for mmWave MIMO systems. Using computer simulations and convergence analysis, the hyperparameter-free MCC is found to be a better channel estimation technique for next-generation communications with impairments due to impulsive noise. This makes the hyperparameter-free MCC a promising solution for channel estimation over practical mmWave MIMO deployments.

Data availability statement

The original contributions presented in the study are included in the article/supplementary material; further inquiries can be directed to the corresponding author.

Author contributions

VB: Software, Formal analysis, Writing – original draft, Conceptualization, Investigation, Writing – review and editing, Methodology. RK: Writing – original draft, Writing – review and editing. RM: Writing – review and editing, Writing – original draft. SJ: Writing – review and editing, Writing – original draft. VS: Writing – review and editing, Writing – original draft. KV: Writing – review and editing, Writing – original draft. OK: Writing – review and editing, Writing – original draft.

Funding

The authors declare that no financial support was received for the research and/or publication of this article.

Conflict of interest

The authors declare that the research was conducted in the absence of any commercial or financial relationships that could be construed as a potential conflict of interest.

The authors declared that they were an editorial board member of Frontiers, at the time of submission. This had no impact on the peer review process and the final decision.

Correction note

A correction has been made to this article. Details can be found at: 10.3389/frsip.2026.1783015.

Generative AI statement

The authors declare that no Generative AI was used in the creation of this manuscript.

Any alternative text (alt text) provided alongside figures in this article has been generated by Frontiers with the support of artificial intelligence and reasonable efforts have been made to ensure accuracy, including review by the authors wherever possible. If you identify any issues, please contact us.

Publisher's note

All claims expressed in this article are solely those of the authors and do not necessarily represent those of their affiliated organizations, or those of the publisher, the editors and the reviewers. Any product that may be evaluated in this article, or claim that may be made by its manufacturer, is not guaranteed or endorsed by the publisher.

References

Ali, S., Saad, W., Rajatheva, N., Chang, K., Steinbach, D., Sliwa, B., et al. (2020). 6G white paper on machine learning in wireless communication networks.

Alkhateeb, A., El Ayach, O., Leus, G., and Heath, R. W. (2014). Channel estimation and hybrid precoding for millimeter wave cellular systems. *IEEE J. Sel. Top. Signal Process.* 8, 831–846. doi:10.1109/jstsp.2014.2334278

Awan, D. A., Cavalcante, R. L. G., Yukawa, M., and Stańczak, S. (2017). Detection for 5G-NOMA: an ooline adaptive machine learning approach. *IEEE Int. Conf. Commun. (ICC)*, 1–6. doi:10.1109/ICC.2018.8422449

Bazzi, A., Slock, D. T., and Meilhac, L. (2016). "Sparse recovery using an iterative variational bayes algorithm and application to AoA estimation," in 2016 IEEE international symposium on signal processing and information technology (ISSPIT) *(IEEE)*, 197–202.

Bazzi, A., Ying, M., Kanhere, O., Rappaport, T. S., and Chafii, M. (2025). ISAC imaging by channel state information using ray tracing for next generation 6G. *IEEE J. Sel. Top. Electromagn. Antennas Propag.* 1, 135–149. doi:10.1109/jsteap.2025.3605877

Bhatia, V., and Mulgrew, B. (2004). "Non-parametric maximum likelihood channel estimation in Non-Gaussian noise," in *IEEE/IEE international workshop on signal processing for wireless communications (SPWC 2004)*.

Bhatia, V., Swami, P., Sharma, S., and Mitra, R. (2019). Non-orthogonal multiple access as an enabler for massive connectivity for 5G and beyond networks. *arXiv Preprint arXiv:1912*. doi:10.48550/arXiv.1912.07077

Chen, B., Zhu, Y., Hu, J., and Principe, J. C. (2013). *System parameter identification: information criteria and algorithms*. London: Elsevier.

Chen, B., Wang, X., Li, Y., and Principe, J. C. (2019). Maximum correntropy criterion with variable center. *IEEE Signal Process. Lett.* 26, 1212–1216. doi:10.1109/lsp.2019.2925692

Chikha, H. B., Alaerjan, A., and Jabeur, R. (2025). Deep learning for enhancing automatic classification of M-PSK and M-QAM waveform signals dedicated to single-relay cooperative MIMO 5G systems. *Sci. Rep.* 15, 26018. doi:10.1038/s41598-025-10738-z

Čirkić, M., and Larsson, E. G. (2014). SUMIS: near-Optimal soft-in soft-out MIMO detection with low and fixed complexity. *IEEE Trans. Signal Process.* 62, 3084–3097. doi:10.1109/TSP.2014.2303945

Cover, T. M., and Thomas, J. A. (1991). Information theory and statistics. *Elem. Information Theory* 1, 279–335. doi:10.1002/047174882X

Elbamby, M. S., Perfecto, C., Bennis, M., and Doppler, K. (2018). "Edge computing meets millimeter-wave enabled VR: paving the way to cutting the cord," in *IEEE wireless communications and networking conference (WCNC)* (IEEE), 1–6.

Forenza, A., Love, D. J., and Heath, R. W. (2007). Simplified spatial correlation models for clustered MIMO channels with different array configurations. *IEEE Trans. Veh. Technol.* 56, 1924–1934. doi:10.1109/tvt.2007.897212

Ghosh, M. (2002). Analysis of the effect of impulse noise on multicarrier and single carrier QAM systems. *IEEE Trans. Commun.* 44, 145–147. doi:10.1109/26.486604

Heath, R. W., Gonzalez-Prelcic, N., Rangan, S., Roh, W., and Sayeed, A. M. (2016). An overview of signal processing techniques for millimeter wave MIMO systems. *IEEE J. Sel. Top. Signal Process.* 10, 436–453. doi:10.1109/jstsp.2016.2523924

Hemadeh, I. A., Satyanarayana, K., El-Hajjar, M., and Hanzo, L. (2017). Millimeter-wave communications: physical channel models, design considerations, antenna constructions, and link-budget. *IEEE Commun. Surv. and Tutorials* 20, 870–913. doi:10.1109/comst.2017.2783541

Kumar, R., Shukla, V. B., Mitra, R., Bhatia, V., Rajatheva, N., and Latva-Aho, M. (2024). "Hyperparameter free information theoretic learning based channel estimation for mmWave MIMO," in *2024 27th international symposium on wireless personal multimedia communications (WPMC)* (IEEE), 1–5.

Ma, W., Qu, H., Gui, G., Xu, L., Zhao, J., and Chen, B. (2015). Maximum correntropy criterion based sparse adaptive filtering algorithms for robust channel estimation under Non-Gaussian environments. *J. Frankl. Inst.* 352, 2708–2727. doi:10.1016/j.jfranklin.2015.03.039

Mitra, R., and Bhatia, V. (2018). Kernel-based parallel multi-user detector for massive-MIMO. *Comput. and Electr. Eng.* 65, 543–553. doi:10.1016/j.compeleceng.2017.02.005

Mitra, R., Miramirkhani, F., Bhatia, V., and Uysal, M. (2018). Mixture-kernel based post-distortion in RKHS for time-varying VLC channels. *IEEE Trans. Veh. Technol.* 68, 1564–1577. doi:10.1109/tvt.2018.2888545

Mitra, R., Kaddoum, G., Dahman, G., and Poitau, G. (2021). Hyperparameter free MEE-FP based localization. *IEEE Signal Process. Lett.* 28, 1938–1942. doi:10.1109/lsp.2021.3111596

Mitra, R., Kaddoum, G., and Da Costa, D. B. (2022). Hyperparameter free MEEF-Based learning for next generation communication systems. *IEEE Trans. Commun.* 70, 1682–1696. doi:10.1109/tcomm.2022.3142138

Rahimi, A., and Recht, B. (2007). Random features for large-scale kernel machines. *Adv. Neural Inf. Process. Syst.* 20. doi:10.5555/2981562.2981710

Saad, W., Bennis, M., and Chen, M. (2019). A vision of 6G wireless systems: applications, trends, technologies, and open research problems. *IEEE Netw.* 34, 134–142. doi:10.1109/mnet.001.1900287

Selim, B., Alam, M. S., Evangelista, J. V., Kaddoum, G., and Agba, B. L. (2020a). NOMA-Based IoT networks: impulsive noise effects and mitigation. *IEEE Commun. Mag.* 58, 69–75. doi:10.1109/mcom.001.1900713

Selim, B., Alam, M. S., Kaddoum, G., and Agba, B. L. (2020b). Effect of impulsive noise on uplink NOMA systems. *IEEE Trans. Veh. Technol.* 69, 3454–3458. doi:10.1109/tvt.2020.2964275

Srivastava, S., Mishra, A., Rajoriya, A., Jagannatham, A. K., and Ascheid, G. (2019). Quasi-static and time-selective channel estimation for block-sparse millimeter wave hybrid MIMO systems: Sparse bayesian learning (SBL) based approaches. *IEEE Trans. Signal Process.* 67, 1251–1266. doi:10.1109/tsp.2018.2890058

Van Zelst, A., and Hammerschmidt, J. (2002). A single coefficient spatial correlation model for multiple-input multiple-output (MIMO) radio channels. *Proc. 27th General Assembly Int. Union Radio Sci. (URSI)*.

Zhang, J. A., Liu, F., Masouros, C., Heath, R. W., Feng, Z., Zheng, L., et al. (2021). An overview of signal processing techniques for joint communication and radar sensing. *IEEE J. Sel. Top. Signal Process.* 15, 1295–1315. doi:10.1109/jstsp.2021.3113120

Zhao, H., Mayzus, R., Sun, S., Samimi, M., Schulz, J. K., Azar, Y., et al. (2013). "28 ghz millimeter wave cellular communication measurements for reflection and penetration loss in and around buildings in New York city," in *2013 IEEE international conference on communications (ICC)* (IEEE), 5163–5167.